Supplementary Information

In situ construction of amorphous hierarchical iron oxyhydroxide nanotubes *via* selective dissolution-regrowth strategy for enhanced lithium storage

Fangyu Xiong,[#1] Fan Lv,[#2] Chen Tang,[1] Pengfei Zhang,[1] Shuangshuang Tan,[1] Qinyou An,[1,3] Shaojun Guo,*[2,4,5] Liqiang Mai*[1]*

[1]Key Laboratory of Advanced Technology for Materials Synthesis and Processing, Wuhan University of Technology, Wuhan, 430070, China.

[2]Department of Materials Science & Engineering, College of Engineering, Peking University, Beijing, 100871, China.

[3]Foshan Xianhu Laboratory, Foshan, 528000, China.

[4]BIC-ESAT, College of Engineering, Peking University, Beijing, 100871, China.

[5]Beijing Key Laboratory for Magnetoeletric Materials and Devices (BKL-MEMD), Peking University, Beijing 100871, China.

[#]These authors contributed equally to this work.

*Corresponding author (email: anqinyou86@whut.edu.cn; guosj@pku.edu.cn; mlq518@whut.edu.cn)

Figure

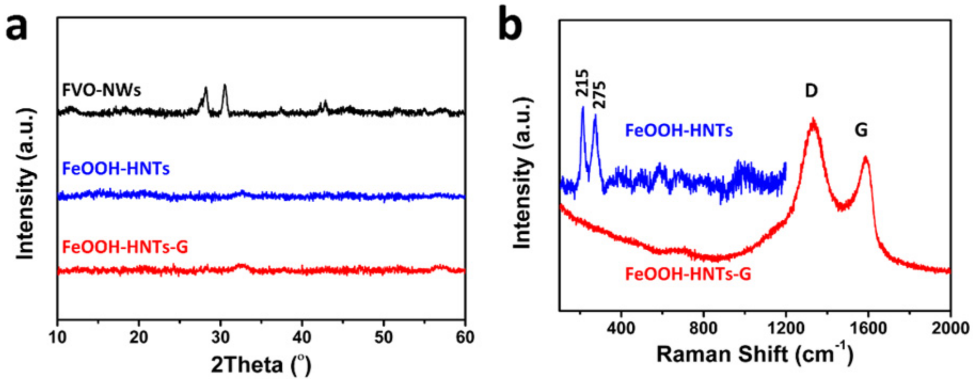

Figure S1. (a) The XRD patterns of FVO-NWs, FeOOH-HNTs and FeOOH-HNTs-G. (b) Raman spectra of FeOOH-HNTs and FeOOH-HNTs-G.

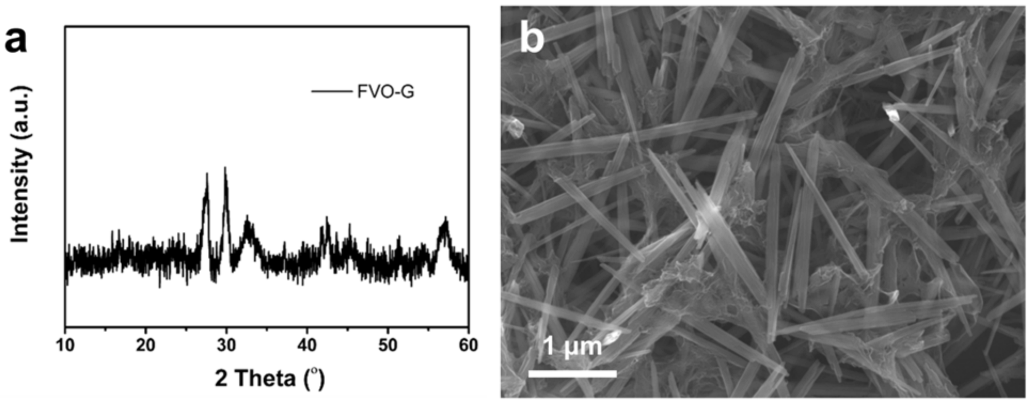

Figure S2. (a) XRD pattern and (b) SEM image of FVO-NWs-G.

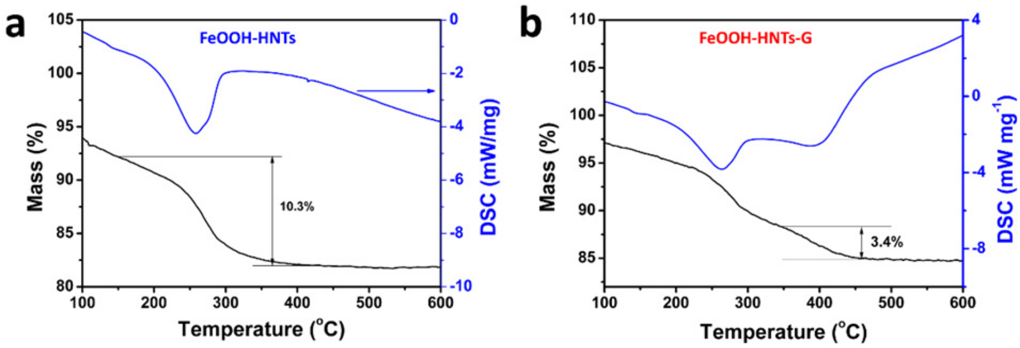

Figure S3. The TG-DSC curves of (a) FeOOH-HNTs and (b) FeOOH-HNTs-G.

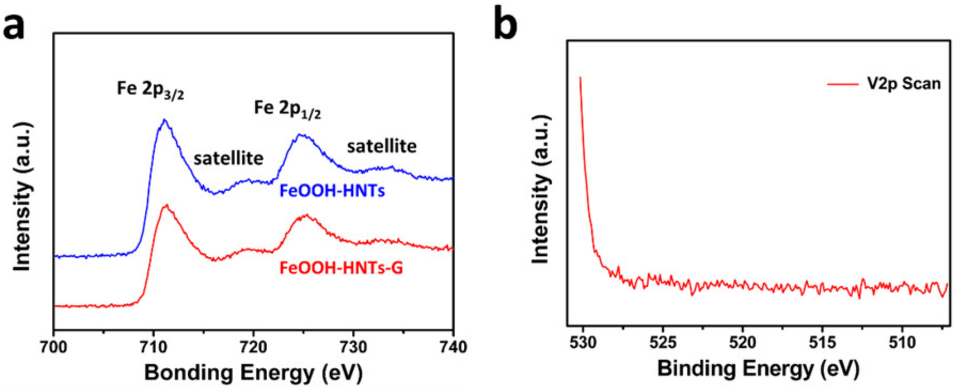

Figure S4. (a) The Fe 2p XPS spectra of FeOOH-HNTs and FeOOH-HNTs-G and (b) V 2p XPS spectrum of FeOOH-HNTs.

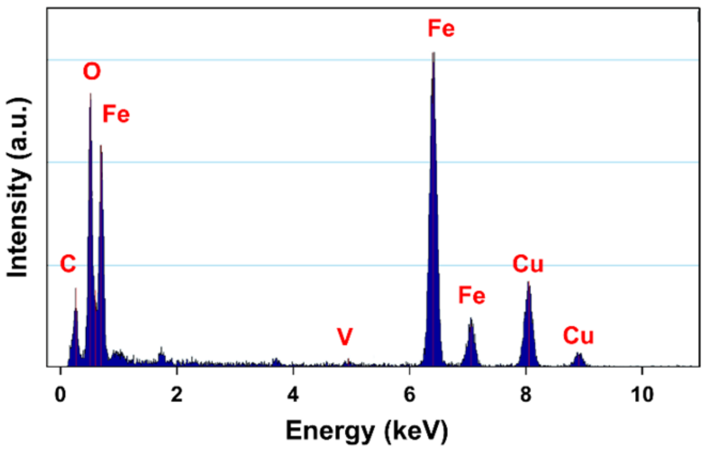

Figure S5. The EDS spectrum of FeOOH-HNTs.

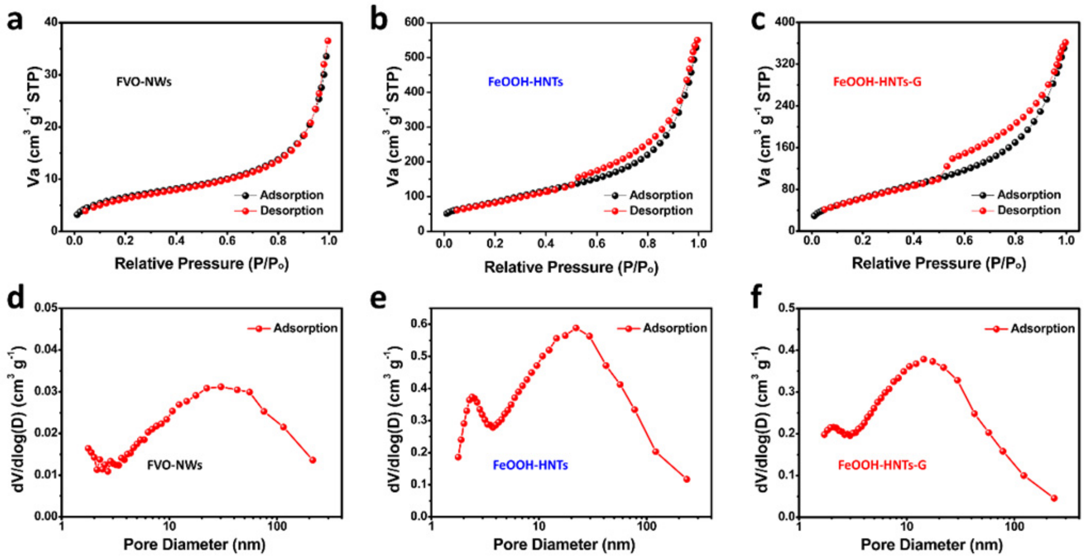

Figure S6. Nitrogen adsorption−desorption isotherms and corresponding pore size distribution plots of (a, d) FVO-NWs, (b, e) FeOOH-HNTs and (c, f) FeOOH-HNTs-G.

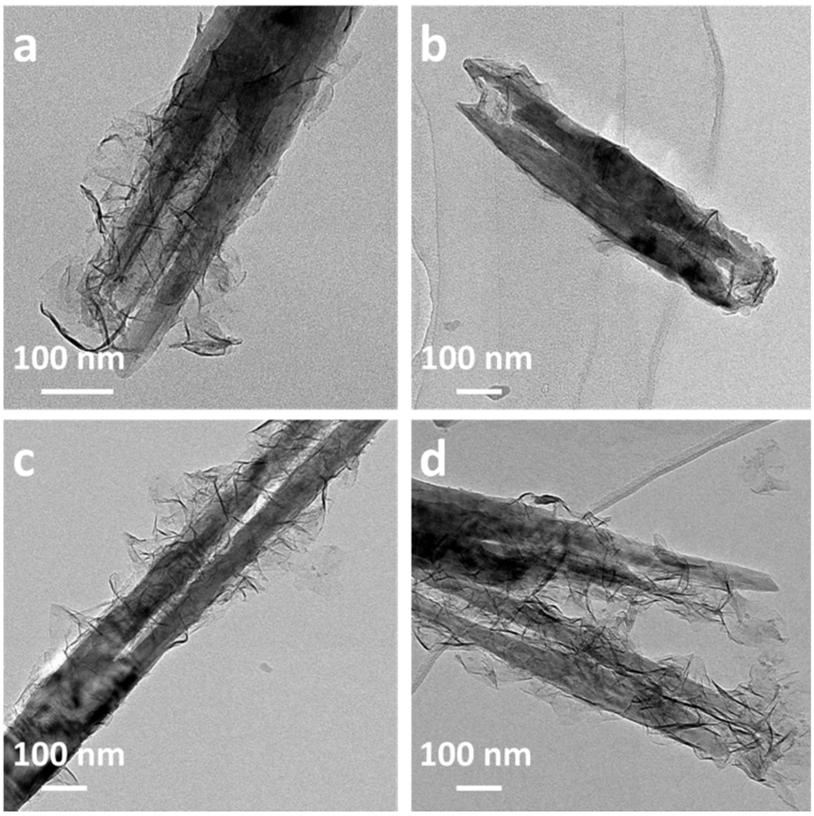

Figure S7. TEM images of sample during transformation from FVO-NWs to FeOOH-HNTs.

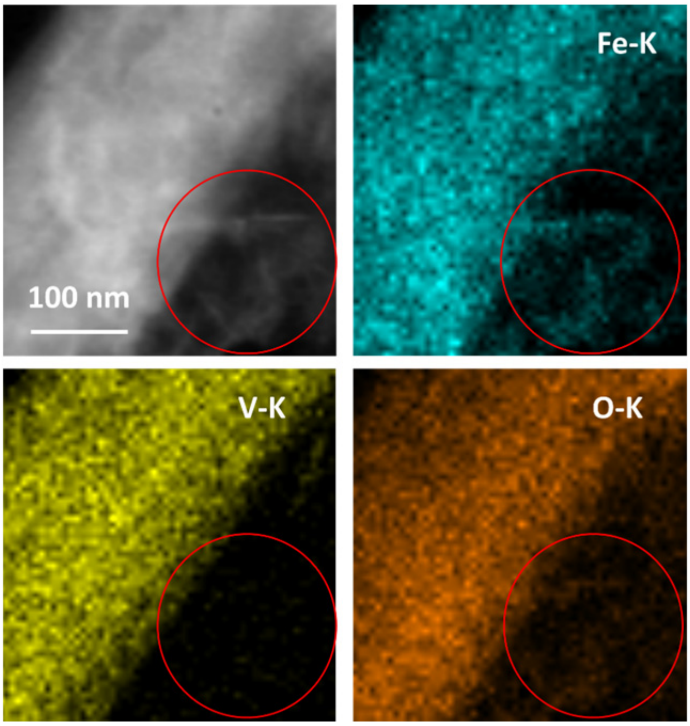

Figure S8. The HAADF image and the EDS elemental mappings of FVO-NWs after treatment with NaOH solution for 20 mins.

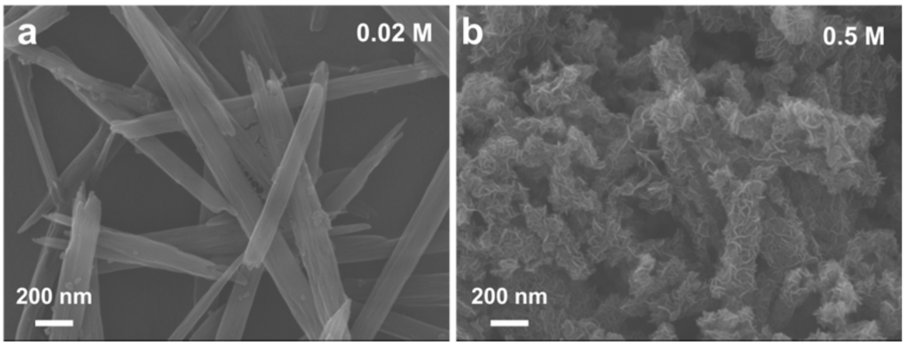

Figure S9. FESEM images of samples obtained from FVO-NWs by etching with (a) 0.02 M and (b) 0.5 M NaOH solution.

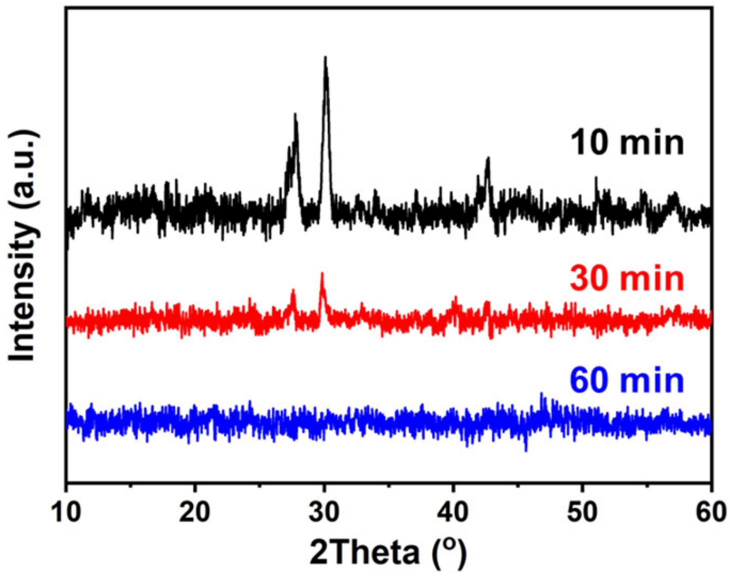

Figure S10. XRD patterns of samples after selective dissolution treatment for different times: 10, 30 and 60 min.

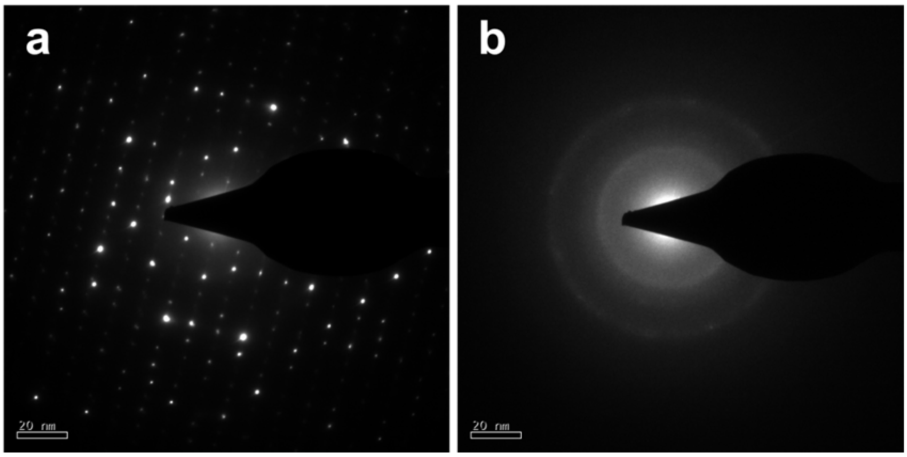

Figure S11. The SAED patterns of (a) FVO-NWs and (b) FeOOH-HNTs.

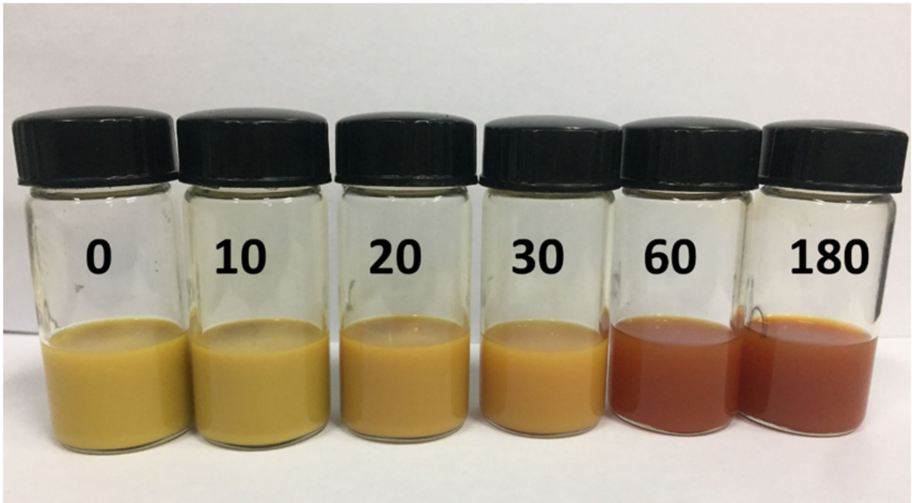

Figure S12. Digital photographs of FVO-NWs treated in NaOH solution for different time (unit: min).

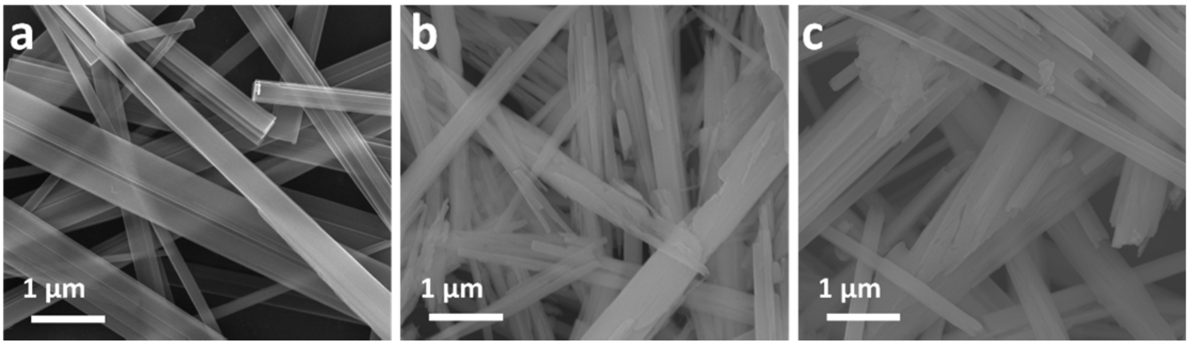

Figure S13. FESEM images of (a) copper vanadate, (b) cobalt molybdate and (c) manganese molybdate nanowires.

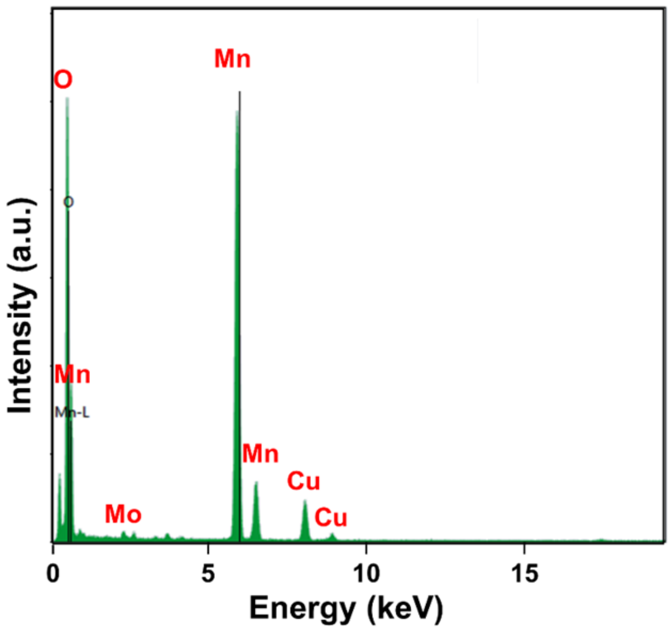

Figure S14. The EDS spectrum of manganese oxide hierarchical nanowires.

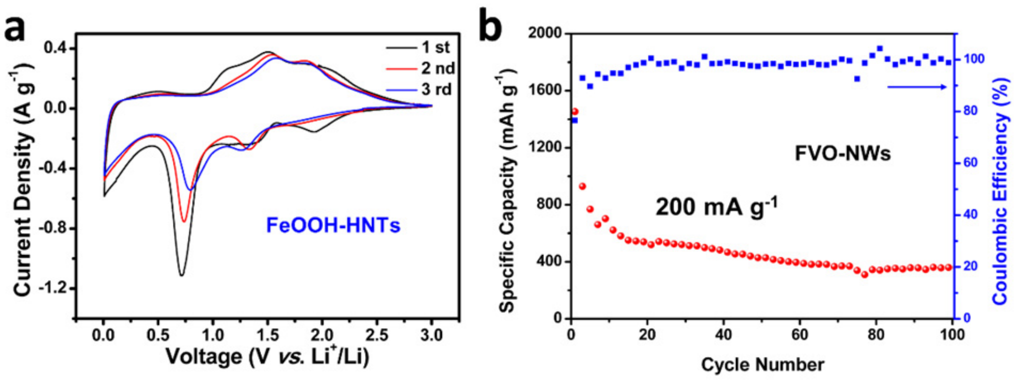

Figure S15. (a) The CV curves of FeOOH-HNTs at 0.1 mV s^{-1} and (b) The cycling performance of FVO-NWs at 200 mA g^{-1}.

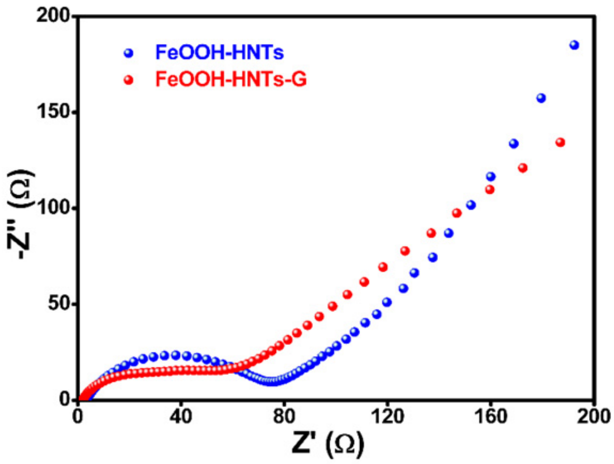

Figure S16. Nyquist plots of FeOOH-HNTs and FeOOH-HNTs-G.

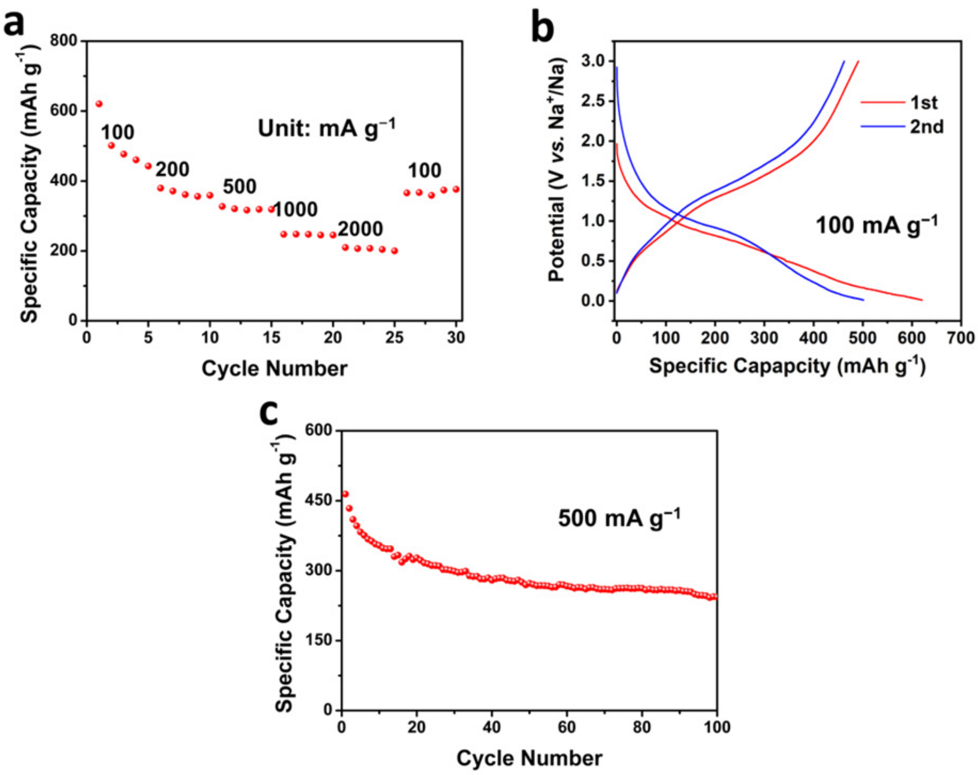

Figure S17. The sodium storage performance of FeOOH-HNTs-G. (a) Rate performance, (b) the corresponding charge/discharge curves at 100 mA g^{-1}, and (c) cycling performance at 500 mA g^{-1}.

Table S1. The comparison for cycling performance of FeOOH-based LIBs anode materials

Materials	Cycle number	Capacity after cycling ($mAh\ g^{-1}$)	Current density ($mA\ g^{-1}$)	Ref.
Amorphous FeOOH/ rGO composites	600	767	1000	S1
Atomically thin γ□FeOOH nanosheets	100	850	200	S2
FeOOH nanorod/ rGO composites	200	1135	1000	S3
β-FeOOH nanorods	600 3500	~700[a] ~600[b]	500 2000	S4
Hexapods α-FeOOH/rGO composites	50	610	100	S5
FeOOH particles/single-walled carbon nanotube composites	180	758	400	S6
β-FeOOH nanorod on carbon cloth	150	~900[c]	1000	S7
β-FeOOH nanorods /graphene composites	100	650	100	S8
Graphene decorated amorphous FeOOH hierarchical nanotubes	900/1800	568/463	1000	This work

[a] The electrode containing 70% *β*-FeOOH and 10% graphite, and the specific capacity is calculated based on the mass of *β*-FeOOH.

[b] The electrode containing 50% *β*-FeOOH and 30% graphite, and the specific capacity is calculated based on the mass of *β*-FeOOH.

[c] The estimated value after subtracting the capacity contribution of carbon cloth.

S1. Sun Y, Hu X, Luo W, et al. Synthesis of amorphous FeOOH/reduced graphene oxide composite by infrared irradiation and its superior lithium storage performance. *ACS Appl Matar Interfaces*, 2013, 5(20): 10145-10150

S2. Song Y, Cao Y, Wang J, et al. Bottom-up approach design, band structure, and lithium storage properties of atomically thin gamma-FeOOH nanosheets. *ACS Appl Matar Interfaces*, 2016, 8(33): 21334-21342

S3. Qi H, Cao L, Li J, et al. High pseudocapacitance in FeOOH/rGO composites with superior performance for high rate anode in li-ion battery. *ACS Appl Matar Interfaces*, 2016, 8(51): 35253-35263

S4. Yu L, Xi S, Wei C, et al. Superior lithium storage properties of β-FeOOH. *Adv Energy Mater*, 2015, 5(6): 1401517

S5 Zhang C, Zhu J, Rui X, et al. Synthesis of hexagonal-symmetry α-iron oxyhydroxide crystals using reduced graphene oxide as a surfactant and their li storage properties. *CrystEngComm*, 2012, 14(1): 147-153

S6. Zou M, Wen W, Li J, et al. Nano-crystalline FeOOH mixed with SWNT matrix as a superior anode material for lithium batteries. *J Energy Chem*, 2014, 23(4): 513-518

S7. Peng S, Yu L, Sun M, et al. Bunched akaganeite nanorod arrays: Preparation and high-performance for flexible lithium-ion batteries. *J Power Sources*, 2015, 296:237-244

Zhang X, Du Y. Gelatin assisted wet chemistry synthesis of high quality β-FeOOH nanorods anchored on graphene nanosheets with superior lithium-ion battery application. *RSC Adv*, 2016, 6(21): 17504-17509